EFFECT OF MEAN STRESS ON THE DAMAGE

OF WIND TURBINE BLADES[*†]

Herbert J. Sutherland
Sandia National Laboratories
Albuquerque, NM 87185-0708
hjsuthe@sandia.gov

and

John F. Mandell
Montana State University
Bozeman, MT 59717
johnm@coe.montana.edu

ABSTRACT

In many analyses of composite wind turbine blades, the effects of mean stress on the determination of damage are either ignored completely or they are characterized inadequately. An updated Goodman diagram for the fiberglass materials that are typically used in wind turbine blades has been released recently. This diagram, which is based on the MSU/DOE Fatigue Database, contains detailed information at thirteen R-values. This diagram is the most detailed to date, and it includes several loading conditions that have been poorly represented in earlier studies. This formulation allows the effects of mean stress on damage calculations to be evaluated. The evaluation presented here uses four formulations for the S-N behavior of the fiberglass. In the first analysis, the S-N curve for the composite is assumed to be independent of mean stress and to have a constant slope. The second is a linear Goodman diagram, the third is a bi-linear Goodman diagram and the fourth is the full Goodman diagram. Two sets of load spectra, obtained by the LIST (Long term Inflow and Structural Test) program, are used for this evaluation. The results of the analyses, equivalent fatigue loads and damage predictions, are compared to one another. These results illustrate a significant overestimation of the equivalent fatigue loads when the mean stress is not considered in the calculation. And, the results from the updated Goodman diagram illustrate that there are a significant differences in accumulated damage when the Goodman diagram

includes information on the transition between compressive and tensile failure modes.

INTRODUCTION

The damage analysis of wind turbine blades requires a detailed description of the fatigue load spectra and the fatigue behavior of blade material. The latter is typically presented as a Goodman diagram in which the cycles-to-failure are plotted as a function of mean stress and range along lines of constant R-values [1]. The R-value for a fatigue cycle is defined as:

$$R = \frac{\sigma_{min}}{\sigma_{max}} \quad , \qquad (1)$$

where σ_{min} is the minimum stress and σ_{max} is the maximum stress in a fatigue stress cycle (tension is considered positive and compression is negative).

As the Goodman diagram is a non-linear function for typical wind turbine blade materials, many analyses completely ignore the effects of mean stress on the determination of damage in composite wind turbine blades. Even when a "complete" Goodman diagram is used, available Goodman diagrams for the fiberglass composite materials typically used in wind turbine blades are relatively sparse with material characterization at only five or six R-values [1-3].

In a recent publication, Mandell et al [4] have presented a detailed Goodman diagram for these fiberglass materials. Their formulation uses the MSU/DOE Fatigue Database [5, 6] to develop a Goodman diagram with information at thirteen R-values. This diagram is

---

the most detailed to date, and it includes several loading conditions that have been poorly represented in earlier studies. This formulation allows the effects of mean stress on damage calculations to be evaluated with greater accuracy.

To illustrate the effect of the updated Goodman diagram on the fatigue analysis of wind turbine blades, the experimentally determined load spectra from the LIST (Long term Inflow and Structural Test) program [7,8] are evaluated using four formulations of the Goodman diagram. In the first analysis, the S-N curve for the composite is assumed to be independent of mean stress and to have a constant slope, a common set of assumptions. The second is a linear Goodman diagram; the third is bi-linear Goodman diagram and the fourth is the detailed Goodman diagram based on the MSU/DoE Database.

The results of these analyses are presented as Equivalent Fatigue Loads, EFL, and damage predictions [1]. The EFL provides a reference for determining the severity of a load spectrum and is used for the accelerated testing of turbine blades. Also, the EFL is a more reliable parameter for comparing fatigue analyses because it is not subject to the extreme variations noted in typical predictions of service lifetimes [1].

For the assumption set used here, the results illustrate a significant overestimate of the EFL and an underestimate of the service lifetime when the mean stress is not considered. And, the results from the updated Goodman diagram illustrate the importance of including information on the transition between compressive and tensile failure modes in the fatigue characterization of fiberglass composites.

S-N FORMULATIONS

The four formulations of the relationship between stress level and number of fatigue cycles to failure, commonly called the S-N relationship, are used in the analysis presented here. These four relationships are described in this section.

Power Law Formulation

One of the simplest formulations for the S-N relationship is a power law formulation. In the normalized form, the power law formulation takes the following form:

$$\sigma/\sigma_o = C_p \, N^{-\frac{1}{m}} \quad , \tag{2}$$

where σ is the alternating stress level of the fatigue cycles, σ_o is the ultimate strength (in either tension or compression), N is the number of cycles to failure, m is the fatigue exponent and C_p is a material constant. In this form, C_p is usually taken to be one. Typical values of m are 3, 6 and 10, which correspond to steel, aluminum and fiberglass composites respectively.

The formulation assumes that the S-N formulation is independent of mean stress. Thus, this relationship holds for all R-values.

Linear Goodman Diagram

A linear formulation of the Goodman diagram is shown in Fig. 1a. For the diagram used here, the experimentally-determined S-N curve for an R-value of −1 is used to define the intercepts of the constant life curves with the vertical axis (note that the vertical axis corresponds to R = −1). These values were derived from the formulation and material constants cited in Eq. 3 and Table I, respectively, see below. The ultimate tensile and compressive strengths were also determined experimentally.

Bi-Linear Goodman Diagram

The bi-linear Goodman diagram is similar to the linear Goodman diagram, except that two experimentally-determined S-N curves (at R values of −1 and 0.1) are used to construct the diagram, see Fig. 1b. Again, these constant life curves at these two R-values were derived from the formulation and material constants cited in Eq. 3 and Table I, respectively.

The MSU/DOE Fatigue Database

Recent efforts [9] to improve the accuracy of spectrum loading lifetime predictions have led to the development of a more accurate fatigue model for fiberglass. The DOE/MSU fatigue database currently contains over 8800 test results for over 130 material systems. The database, which is updated annually, is available on the Sandia website [http://www.sandia.gov/wind/]. Refs. 5 and 6 provide a detailed analysis of data trends and blade substructure applications; substructure applications are also addressed in Ref. 10.

The S-N data for the various R-values, see Fig. 1c, were fit using Eq. 3, see below. The results of these fits are summarized in Table I. These data refine the earlier Goodman diagrams [5, 6, 9] for R-values involving
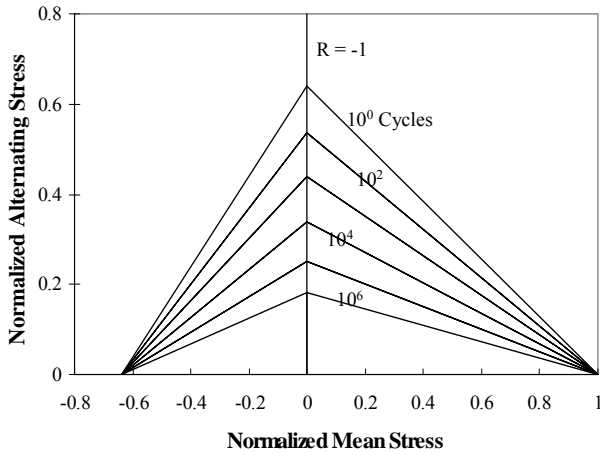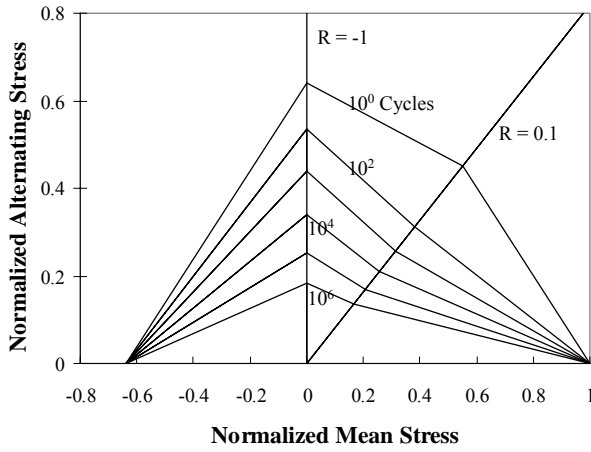
Fig. 1a. Linear Goodman Diagram.

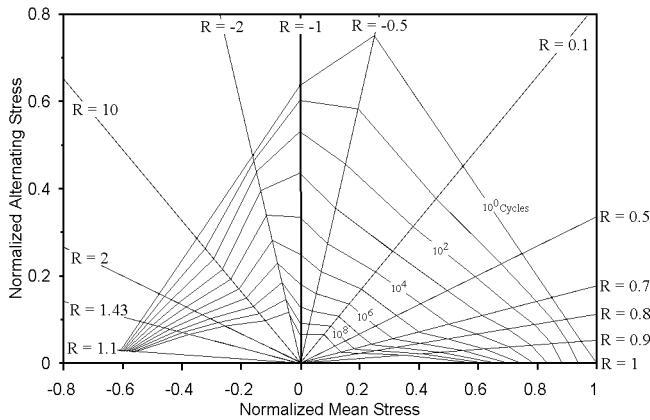**Fig. 1b. Bi-Linear Goodman Diagram.**

Fig. 1c. MSU/DoE Goodman Diagram for Thirteen R-Values for Database Material DD16, Fit with Equation 3.

Table I. Equation 3 Parameters for the Thirteen R-Values for Material DD16 and for Small Strands.

R-Value	Model (Equation 2)		
	a	b	c
1.1	0.060	3.0	0.05
1.43	0.060	3.0	0.15
2	0.060	4.0	0.25
10	0.100	4.0	0.35
−2	0.010	4.0	0.55
−1	0.020	3.0	0.62
−0.5	0.450	0.85	0.25
0.1	0.420	0.58	0.18
0.5	0.075	2.5	0.43
0.7	0.04	2.5	0.45
0.8	0.035	2.5	0.40
0.9	0.060	2.5	0.28
1*	0.21	3.0	0.14

*Assumes a frequency of 10 Hz.

reversed loading, −2, −1 and −0.5, as well as high tensile R-values, 0.7 to 1.0, see Fig. 1c. The high tensile R-value data, in particular, produce a significantly more conservative Goodman diagram in this range, which may improve spectrum-loading predictions.

S-N Models

Many of the R-values shown in Fig. 1c produced semi-log stress versus log cycles S-N trends with complex shapes, relatively flat at low cycles, steeper at medium cycles, and less steep again at high cycles. Mandell et al [10] found that at least three parameters were needed to fit these trends. The particular model used here is given by.

$$\sigma_O - \sigma = a\sigma \left[\frac{\sigma}{\sigma_O} \right]^b (N^c - 1) \qquad (3)$$

where σ is the maximum applied stress, σ_O is the ultimate tensile or compressive strength (obtained at a strain rate similar to the 10 Hz fatigue tests), and a, b, and c are the fitting parameters.

The S-N data for the various R-values are summarized in Fig. 1c. In this figure, the

constant R-value S-N curves plot along radial lines. The new data refine the earlier Goodman diagrams [5, 6, 9] for R-values involving reversed loading, –2, –1 and –0.5, as well as high tensile R-values, 0.7 to 1.0. The high tensile R-value data, in particular, produce a much more conservative Goodman diagram in this range, which may improve spectrum loading predictions.

EXPERIMENTAL LOAD SPECTRA

To evaluate the effects of the improved Goodman diagram on damage calculations requires a detailed knowledge of the load (and stress or strain) spectra.

The LIST (Long-term Inflow and Structural Test) program has obtained long-term load spectra for two turbines. The first is a three-bladed Micon 65/13M wind turbine. This turbine is being tested at a USDA site located near Bushland, Texas, see Fig. 2. This site is representative of most Great Plains commercial sites. For a complete description of the turbine, its instrumentation and the site, see Sutherland, et al. [7]. Sutherland [8] has reported on other analyses of these data. These data have been expanded by Sutherland, et al. [11].

The second turbine is the ART (Advanced Research Turbine), see Fig. 3. It is a Westinghouse 600-kW wind turbine that is currently located at the National Wind Technology Center (NWTC) near Boulder, Colorado. Under the auspices of the LIST program, Kelley et al. [12] collected a long-term data set that includes both the dynamic response of the turbine and detailed inflow measurements. Sutherland, Kelley and Hand [13] have reported an analysis of these data.

The Bushland Turbine

The Turbine

The LIST turbine in Bushland is a Micon 65/13M, see Fig. 2. This fixed-pitch turbine has a 3-phase 480V asynchronous generator, and the turbine is rated at 115 kW. The generator operates at 1200 rpm while the blades turn at a fixed 55 rpm (the standard Micon 65/13 turbine rotates at a fixed 45 rpm). It has a rated wind speed of approximately 15 m/s.

Fig. 2. The Micon 65/13M turbine at the Bushland Test Site.

Fig. 3. The ART at the NWTC.

The turbine is fitted with Phoenix 8m blades that are based on Solar Energy Research Institute (SERI)[**] airfoils. These "SERI" blades are 7.9 m (312 in) long and are equipped with tip brakes. The physical characteristics of these fiberglass blades were obtained from Jackson and Zuteck [14].

Load Spectra

The load spectra obtained in the LIST measurement campaign in Bushland contains 4254 ten-minute records. For all of these records, the turbine is operating for the entire record, the mean wind speed of the record is greater than 7 m/s and the inflow measurements are not blocked. The distribution of these records is summarized in Fig. 4. As illustrated in this figure, 1170 records are above 11 m/s mean wind speed. The records in the ">17" bin contains 20 records above 19 m/s. The highest mean wind speed recorded for a 10-minute data record is 20.2 m/s.

These wind speed bins are used for the analysis presented here. For this analysis, the bins encompassed speed ranges of 7-9, 9-11, 11-13, 13-15 and 15-17 m/s. The final bin encompasses all wind speeds above 17 m/s and the first bin contains all wind speeds below 9 m/s.

A typical fatigue load spectrum from these data is shown in Fig. 5.

The ART

The Turbine

The Westinghouse 600-kW wind turbine [12] is an upwind, two-bladed teetered-hub machine, see Fig. 3. It has full span pitch control and a synchronous generator. The turbine has a rotor diameter of 42 m (137.8 ft.) and a hub height of 36.6 m (120 ft). The turbine is a constant speed machine (43 rpm) that reaches rated power at 12.8 m/s (28.6 mph). Its cut-in wind speed is 6.25 m/s (14 mph) and its cutout wind speed is 22.3 m/s (50 mph). In order to maintain turbine operation at higher wind speeds, the pitch control system was adjusted to marginally increase the cutout wind speed mid-way through the wind season.

The turbine blades are constructed from a *wood/epoxy laminate*. They have a modified LS(1)-04XX airfoil with a nonlinear, 6.75° twist and no pre-cone angle. The first (cantilever) bending frequency of the blade when mounted to the hub is 2.24 Hz in the flapwise direction and 4.56 Hz in the edgewise direction. The
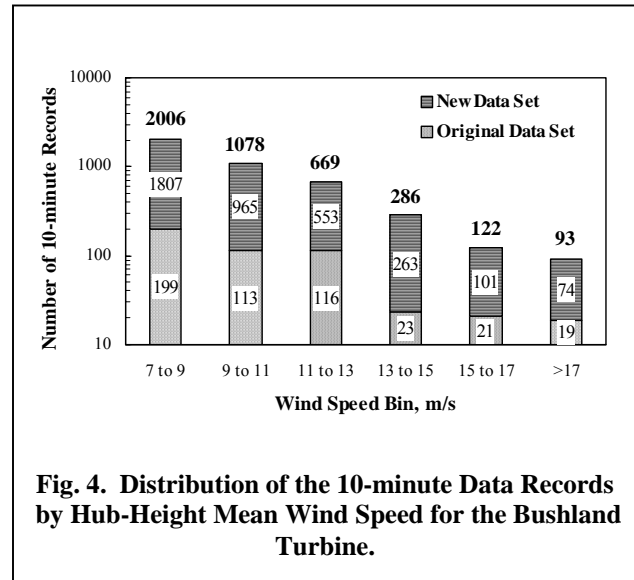
Fig. 4. Distribution of the 10-minute Data Records by Hub-Height Mean Wind Speed for the Bushland Turbine.
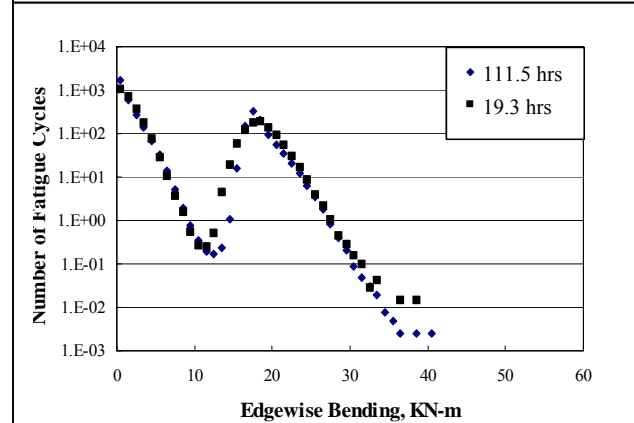

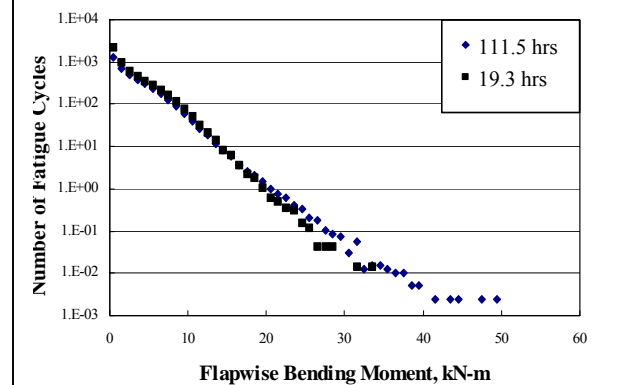**Fig. 5a. Edge-Bending in the Root of Blade 1.**

Fig. 5b. Flap-Bending in the Root of Blade 1.

Fig. 5. Fatigue Load Spectrum for the 11-13 m/s Wind Speed bin for the Bushland Turbine.
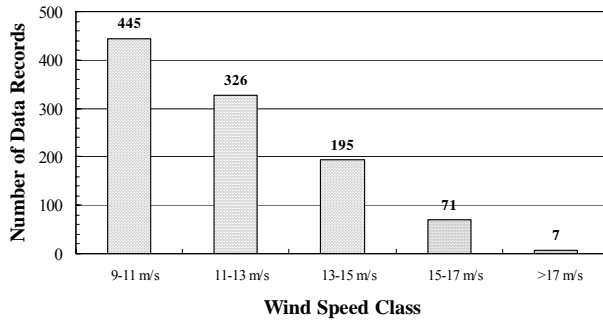
Fig. 6. Distribution of Data Records Used in the Analysis by Wind Speed Bin for the ART.
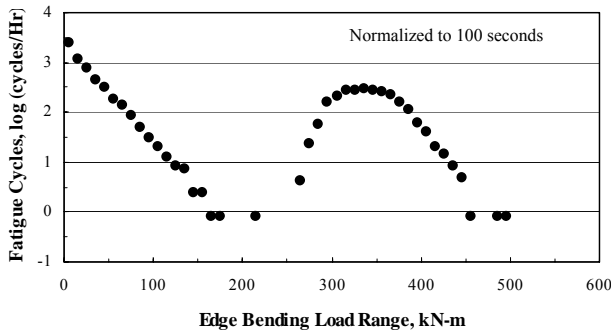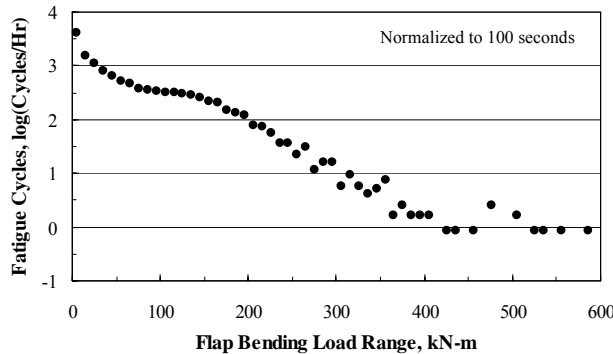

Fig. 7a. Edgewise Bending Moment.

Fig. 7b. Flatwise Bending Moment.

Fig. 7. Typical Fatigue Spectra for Root Bending Moments, >17 m/s Wind Speed Bin for the ART.

shaft is mounted at a tilt angle of 4°. The physical characteristics of these blades were obtained from Malcolm [15].

Load Spectra

The load spectra obtained in the LIST measurement campaign on the ART contains a total of 1044 10-minute records. For all of these records, the turbine operated throughout the duration of the record, the mean wind speed was greater than 9 m/s, and the mean wind direction remained within ±45º of the perpendicular to the planar array. These records were binned by hub-height mean wind speed into bins that were typically 2 m/s. The wind speed bins 9-11, 11-13, 13-15, 15-17, and >17 m/s are considered here. The number of records contained in each bin is 445, 326, 195, 71 and 7, respectively, see Fig. 6. The maximum mean wind speed in the >17 wind speed bin is 17.4 m/s.

A typical fatigue load spectrum from these data is shown in Fig. 7.

BLADE STRESS LEVELS

To apply the Goodman diagrams shown in Fig. 1 to the loads data shown in Figs. 5 and 7, the loads must be converted to stress or strain levels. This conversion was accomplished using the geometric and material information provided by Jackson and Zuteck for the Bushland turbine [14] and by Malcolm for the ART [15].

The total stress level in the blade root σ is composed of two parts: (1) the bending stress σ_B associated with the aerodynamic forces and gravity and (2) the axial stress σ_T associated with the centrifugal load created by the rotation of the blade. Namely,

$$\sigma = \sigma_B + \sigma_T \quad . \tag{4}$$

In terms of the bending moment F_B, Eq. 4, takes the form:

$$\sigma = \pm C_B F_B + \sigma_T \quad . \tag{5}$$

The constant C_B that relates the bending stress σ_B to the bending moment F_B is a function of the root geometry and root material properties. The ± sign associated with this term reflects the compressive and tensile sides of the bending stress in the outer

fibers of the root.

The rotation tension term σ_T is a function of the blade weight, location of the center-of-gravity, rotational speed, the area of the root and root material properties. As both turbines analyzed here are constant speed turbines, this term is constant.

Equation 5 is used here for both the flapwise and edgewise loads.

As this technique yields nominal stress, a stress concentration factor was applied to convert the nominal stress level to the actual strress level. This conversion factor was chosen to yield a maximum root strain of 0.3 percent strain.

The blades on the ART are constructed from wood laminate. And, the S-N formulations cited above are for a fiberglass composite. Thus, the two are not compatible. However, for illustrative purposes, we assume that the ART is fitted with an equivalent fiberglass blade for the ART that has the same physical dimensions and strain levels as its wood counterpart.

DAMAGE CALCULATIONS

To illustrate the significance of the updated material properties shown in Fig. 1c, damage calculations are used. The results of these formulations are reported in two forms, both of which are based on Miner's Rule. The first form is a determination of damage using the predicted service lifetime and the second is the Equivalent Fatigue Load (EFL).

Prediction of Damage

The load spectra cited are composed of a series of bending load cycles n_{ij} that are binned by their range and mean. namely,

$$n_{ij} \equiv n_{ij}\left(F_m , F_R\right) \quad , \qquad (6)$$

where F_m and F_R are the mean and range (amplitude) components of the fatigue load cycles. The CRUNCH code [16] was used for this binning analysis. In stress space, Eq. 6 can be rewritten using Eq. 5 to yield

$$\begin{aligned} \sigma_{ij} &= \sigma_{ij}\left[\sigma_m , \sigma_R\right] \\ &= \sigma_{ij}\left[\left(C_B F_M\right)+\sigma_T , \left(C_B F_R\right)\right] \end{aligned} \qquad (7)$$

Using the definition of R-value cited in Eq. 1, the fatigue cycles can be re-binned into R and range bins, namely,

$$n_{ij}\left(\sigma_m , \sigma_R\right) \Rightarrow n_{kl}\left(R , \sigma_R\right) \quad . \qquad (8)$$

Then, Miner's rule defines the damage **D**, predicted for a time interval T, as

$$D = \sum_k \sum_l \frac{n_{kl}\left(R, \sigma_R\right)}{N\left(R, \sigma_R\right)} \quad . \qquad (9)$$

Failure occurs when **D** equals one. The predicted service lifetime **L**, is the time T required for the damage **D**(T) to accumulate to a value of one.

Equivalent Fatigue Load

Then, the Equivalent Fatigue Stress, EFS, σ_e is defined as the cyclic stress level that will product a specified damage **D** in a specified number of fatigue cycles N_o. Thus, the EFS for the spectra $n_{kj}(R, \sigma_R)$, see Eq. 9, may be written as [1]:

$$\frac{N_o}{N\left(-1, \sigma_e\right)} = \sum_k \sum_l \frac{n_{kl}\left(R, \sigma_R\right)}{N\left(R, \sigma_R\right)} \quad . \qquad (10)$$

For formulation, $N(R, \sigma_R)$ is defined by the four S-N formulations cited above.

The choice of N_o is somewhat arbitrary. It is sometimes chosen to be a number of cycles suitable for laboratory testing, i.e., 10^6 cycles [17]. Other times, it is chosen to be approximately the average number of cycles recorded in the data set; i.e., the average number of cycles in a 10-minute data set. If data are not available, then the choice of N_o is typically based upon the rotational frequency f_o of the turbine [17]. Since the choice of N_o is essentially arbitrary and does not influence the comparative nature of the analysis presented here, we will assume a constant value for N_o of 2000 cycles for the equivalent-fatigue-load data analyses of a 10-minute record and 10^6 cycles for the lifetime analyses.

As noted in Eq. 10, the equivalent fatigue stress is determined for $R = -1$.

Goodman Diagram

For the three Goodman diagrams cited above, the EFS was determined using an iterative numerical solution technique on a mathematical description of the Goodman diagrams; e.g., Eq. 3 and Table I.

Once σ_e is determined, then Eq. 5 can be used to convert from the EFS to the EFL.

Power Law Formulation

The power law formulation of the S-N curve with a fatigue exponent of m, see Eq. 2, may be substituted directly into Eq. 10. Noting that under this formulation the variables are no longer dependent on R, one may show [1, 17] that Eq. 10 reduces to:

$$F_e = \left[\frac{\sum_i \left(F_i\right)^m n_i}{N_o} \right]^{1/m}, \qquad (11)$$

where F_e is the EFL for the load spectra. Note, that under these assumptions, the EFL can be determined without knowing the values for constants C_B and σ_T defined by the load components F_i.

RESULTS AND DISCUSSION

The analysis described in the preceding section of this paper was conducted on the LIST data from both the Bushland turbine and the ART using the Goodman diagrams shown in Fig. 1.

The four S-N models are compared on two bases: EFL and damage (service lifetime). In the initial comparison, the EFL for each wind speed bin are compared to one another. The load spectra from wind speed bins are then summed to form an annual load spectrum. The annual EFL and predicted service lifetime are then compared. For the former comparison, the EFL is based on a N_o of 2000 cycles and for the latter it is based on 10^6 cycles.

While the comparisons to the power law formulation, see Eqs. 2 and 11, cited here have some very important implications, the reader is cautioned against drawing a broad interpretation from these comparisons. In particular, the power law formulation is not dependent on the mean stress. Thus, the EFL at R = −1 (reverse tension and compression) and R = 0.1 (all tensile loads)

are the same for this formulation. This result is not consistent with experimentally determined S-N curves for fiberglass composites because the failure mode for fiberglass is different in compression than it is in tension. Thus, the comparisons are almost like comparing "apples to oranges." To minimize any discrepancies, all of the comparisons presented here are based an R-value of −1 and to the ultimate compressive strength. Comparisons to other R-values will have different results.

Variation with Wind Speed

The results of the EFL analyses of the 10-minute records at the various wind speed bins are summarized in Figs. 8, 9 and 10. These EFL are based on a N_o of 2000 cycles.

The comparison of the four models in Figs. 8 and 9 indicates that there is a major difference between the power law model (Eq. 2) and Goodman diagrams (Fig. 1). In particular, the power law model (Eq. 11 with m = 10) predicts a significantly higher EFL at all values of wind speeds for both turbines. The linear and bi-linear Goodman diagrams (Figs. 1a and 1b, respectively) predict similar EFL, while the MSU/DoE database model (Fig. 1c) predicts a relatively small decrease in the EFL from the other two Goodman diagrams for three of the four load spectra. For the fourth spectra (Fig. 8b), the MSU/DoE model predicts similar results.

The comparison of the edgewise and flapwise EFL for the tension and the compression bending sides are shown in Fig. 10. The data presented in both figures is derived using the MSU/DoE model. As shown in Fig. 10b, the effect of the mean stress on the EFL is relatively small for most wind speeds for the ART load specta, but is relatively more important for all wind speeds for the Bushland turbine. For the ART load spectra, the difference is essentially zero for all bins expect for highest wind speed bin where the difference is approximately 7 percent. For the Bushland turbine, the difference ranges as high as 65 percent (for the highest wind speed bin) for the flapwise bending direction and as high as 21 percent for the edgewise spectra. The tensile flapwise spectra are more damaging than the compressive spectra, and the compressive edgewise spectra are more damaging than the tensile spectra.
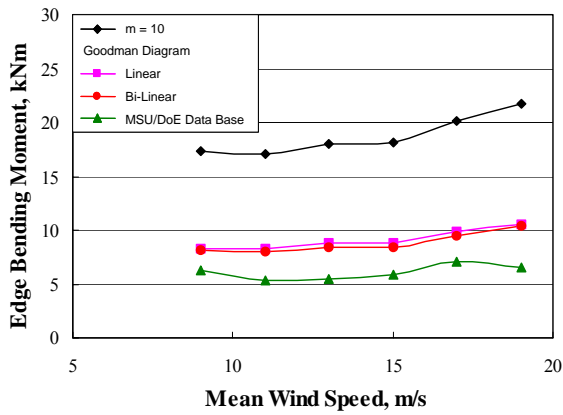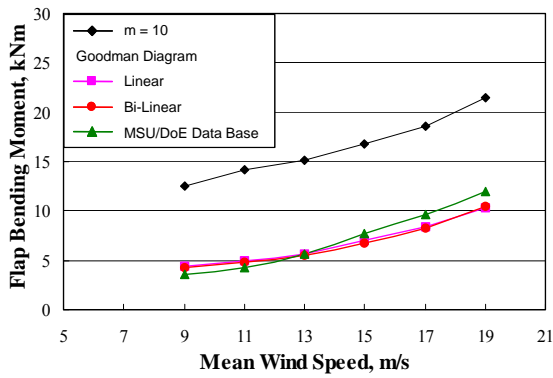
Fig. 8a. Edgewise Bending Moment.

Fig. 8b. Flapwise Bending Moment.

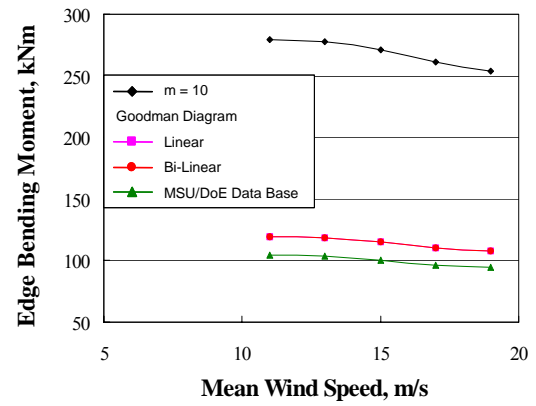**Fig. 8. Equivalent Fatigue Loads for the LIST Turbine on the Tensile Bending Side.**

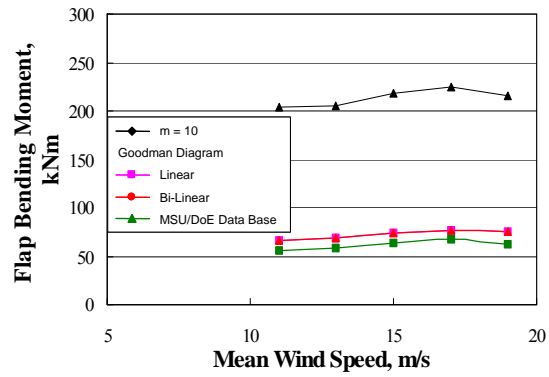**Fig. 9a. Edgewise Bending Moment.**

Fig. 9b. Flapwise Bending Moment.

Fig. 9a. Equivalent Fatigue Loads for the ART on the Tensile Bending Side.
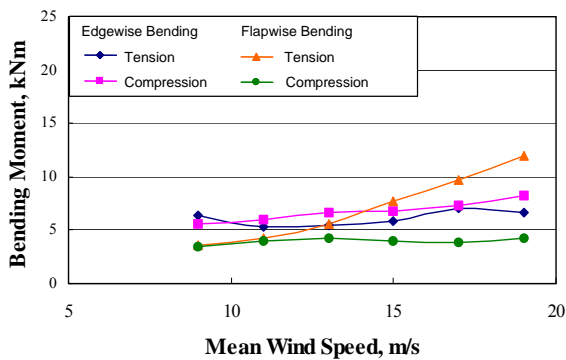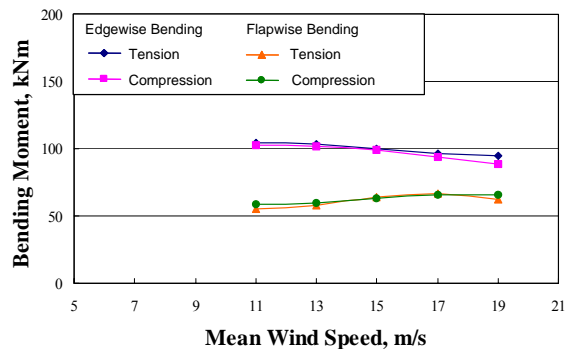

Fig. 10a. EFL for the Bushland Turbine.

Fig. 10b. EFL for the ART.

Fig. 10. Comparison of the EFL on the Tensile and Compressive Sides for the MSU/DoE Goodman Diagram.

Table II. Predicted Service Lifetime for a Rayleigh Wind Speed Distribution using the MSU/DoE Goodman Diagram.

Turbine	Bending Direction	Tension	Compression
Bushland	Edge	1087	938
	Flap	703	19950
ART	Edge	106	118
	Flap	4626	3826

Table III. Predicted Equivalent Fatigue Load for a Rayleigh Wind Speed Distribution using the MSU/DoE Goodman Diagram.

Turbine	Bending Direction	Tension	Compression
Bushland	Edge	9.7	9.9
	Flap	10.4	6.2
ART	Edge	150.8	148.3
	Flap	85.5	88.0

Comparison on an Annual Basis

While the EFL over the wind speed bins are important, an enhanced picture of the implications of the four S-N formulations may be obtained by examining the damage estimates and EFL on an annual basis. For this analysis, the annual load spectrum is constructed from the individual spectra by using a weighted summation based upon a Rayleigh wind speed distribution with a 6.3 m/s (14 mph) mean. The service lifetimes and the EFL were then computed for each of the four S-N formulations. The results of these calculations are summarized in Tables II, III IV and V. The predicted service lifetimes cited in Table II are predictions based on the MSU/DoE Goodman diagram. For Table III, the EFL was computed using an N_o of 10^6 cycles. The results listed in Tables IV and V are normalized to the results listed in Tables II and III, respectively.

Table II illustrates that the flapwise bending on the tension side is critical load state, from damage stand point, for the Bushland turbine and the edgewise bending on the tensile side is critical for the ART. These critical states also produces the largest EFL, see Table III.

For the Bushland turbine, Fig. 10a shows relatively large difference between the compression and tension sides for flapwise bending. This trend is

Table IV. Normalized Predicted Service Lifetime for a Rayleigh Wind Speed Distribution.

Turbine	Bending Direction	Tension				Compression			
		m = 10	Linear	Bi-Linear	Database	m = 10	Linear	Bi-Linear	Database
Bushland	Edge	0.001	0.104	0.128	1.000	0.001	0.124	0.148	1.000
	Flap	0.006	1.879	2.065	1.000	0.000	0.071	0.072	1.000
ART	Edge	0.000	0.414	0.407	1.000	0.000	0.368	0.361	1.000
	Flap	0.000	0.349	0.342	1.000	0.000	0.424	0.424	1.000

Table V. Normalized Equivalent Fatigue Load for a Rayleigh Wind Speed Distribution.

Turbine	Bending Direction	Tension				Compression			
		m = 10	Linear	Bi-Linear	Database	m = 10	Linear	Bi-Linear	Database
Bushland	Edge	2.87	1.40	1.36	1.00	2.81	1.37	1.33	1.00
	Flap	2.13	0.91	0.90	1.00	3.54	1.50	1.49	1.00
ART	Edge	3.02	1.14	1.14	1.00	3.07	1.16	1.16	1.00
	Flap	3.61	1.17	1.18	1.00	3.50	1.14	1.14	1.00

reflected in large difference is predicted service lifetimes shown Table II and in the EFL shown in Table III. However, the lifetime predictions show a difference of over 25 percent. For the ART, the difference between the compression and tension bending sides is more pronounced. For the ART, Tables II and III illustrate that the edgewise load spectrum is the most severe, with the tension bending side being slight more critical than the compressive bending side.

Tables IV and V illustrate that the power law formulation yields the highest EFL and the lowest life. Thus, the power law formulation is always the most severe. Again, the reader should not place a broad interpretation on the magnitude of the difference between the EFL predicted by the power formulation and the Goodman formulations. The difference is a strong function of the R-value used in the analysis of the three formulations of the Goodman diagrams.

In general, the linear and bi-linear Goodman diagrams yield similar EFL and service lifetimes. For all of the cases except one, the MSU/DoE Goodman diagram yields service lifetime predictions that are significantly higher than the linear and bi-linear formulations, and, equivalently, lower EFL. For the Bushland flapwise load spectra on the tensile bending side, the linear and the bi-linear Goodman diagram yields predictions that are only slightly lower from that predicted by the MSU/DoE Goodman diagram.

Data Trends

The trends in the data cited above to appear to be somewhat contradictory at first glance. However, a close examination of the load spectra and the different Goodman formulations do bring some understanding to these results. For the load spectra examined here, most of the fatigue load cycles are clustered around the R= –1 axis. This area of the Goodman diagram is very important because this is the region where the fiberglass composite is in transition between compressive and tensile failure modes. The effect of the mode change on fatigue properties is illustrated by the direct comparison of the constant life curves for the three Goodman diagrams shown Fig. 11. In this figure, the constant life curves for the three formulations of the Goodman diagram at 10^5 cycles are compared to one another. Four distinct regions of comparison are noted: (1) the region of relatively high compressive mean stress (to the left of R = –10); (2) the region of relatively low compressive stress (between R = –10
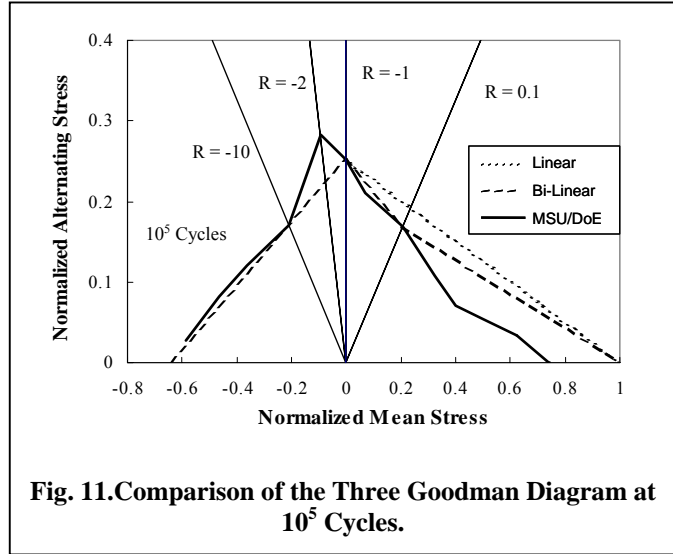

Fig. 11.Comparison of the Three Goodman Diagram at 10^5 Cycles.

and R = –1); (3) the region of relatively low tensile stress (between R = –1 and R = 0.1); and (4) the region of relatively high tensile stress (to the right of R = 0.1). In the first and third regions, the three formulations lie close to one another. Thus, each of the three formulation will predict approximately the same damage rate for the stress cycles in this range. For the fourth region (high tensile stress) the database formulation is below the linear and bi-linear formulations. Thus, the database formulation is more severe (i.e., shorter predicted service lifetime and higher EFL) than the other two. And, finally, for the second region (low compressive stress), the database formulation is above the linear and bi-linear formulations. Thus, it is less severe. Regions 2 and 3 are where the composite is in transition between compressive and tensile failure modes.

For both turbines, most of the fatigue cycles are congregated about the R = –1 axis in regions 2 and 3. Thus, the transition between failure modes governs the predictions. For the ART, the service lifetime predictions for linear and bi-linear formulations are below the database formulations, see Table III. This implies (verified by a detailed examination of the stress cycles) that the spectra are dominated by region 2 cycles. The same is true for the Bushland turbine in edgewise bending and on the compressive side of flapwise bending. However, on the tensile side of flapwise bending, the mean stress is sufficient to move the dominating fatigue cycles from region 2 into region 3 and 4.

Sensitivity

Predictions of service lifetime are notoriously sensitive to minor changes in the fatigue analysis. The results presented here are no exception.

As discussed above, the two load spectra used here were derived from experimental data. The data was cycle counted with CRUNCH [16] which produces a cycles count matrix based on the mean and amplitude of each cycle. In our initial analysis, this 50-by-50 matrix was reduced to a 13-by-50 matrix (R value and amplitude). These values were used in Eq. 9, to compute the damage. This technique for evaluated Eq. 9, while technically correct, yielded different results then those presented here. In particular, this technique lumped many of the region 2 cycles into the R = –1 bins. Thus, their damage contribution was over estimated, and the database formulation produced shortened service lifetimes and higher EFL than the linear and the bi-linear formulations. Equivalent figures to those presented in Figs. 8 and 9, show the database formulation lying above the linear and bi-linear formulations.

For the data presented here, the 50-by-50 matrix was retained. For each bin, Eq. 9 was evaluated by using the mean and amplitude of the stress cycles to determine its R-value. Then, the two closest surrounding R-values were used with the linear constant-line formulation, see Fig. 1, to predict damage. This procedure tracked the description of region 2 more closely.

Obviously, the 50-by-50 matrix calculations are numerically more precise than the 13-by-50 matrix calculations. However, the real question is whether or not the added precision is warranted. The reader is referred to the original S-N data, see Ref. 4, used to construct the numerical descriptions cited in Table VI. The authors' analyses of these data show the behavior illustrated in Fig. 11 and, in their estimation, are a true depiction of the composite's fatigue behavior.

Significant sensitivity to materials variations can also be expected. Figure 1c is derived from mean lifetime values for a particular E-glass/polyester laminate [9]. Variations in fiber content, reinforcing fabric, laminate lay-up, resin system, environment, and statistical treatment could cause significant changes to particular segments of the Goodman diagram [6]. While the use of normalized stress in Figure 1c allows for adjustment to materials with different static strengths, it is evident that fatigue tests must be conducted on a new material at several R-values to validate or modify the trends in Figure 1c.

CONCLUSIONS

The effect of mean stress on the prediction of damage from typical wind turbine load spectra is analyzed using a detailed Goodman diagram for characterizing the behavior of typical fiberglass composites used in wind turbine blades. A detailed formulation of the S-N behavior of these composites is obtained by constructing a Goodman diagram using S-N curves at thirteen different R-values. The data used in this process is contained in the MSU/DoE fatigue database for composite materials. This diagram is the most detailed to date, and it includes several loading conditions that have been poorly represented in earlier studies.

The analysis illustrates the effect of mean stress by comparing damage predictions from the detailed Goodman diagram to three other formulations of the S-N behavior of the fiberglass composite. The other three are a power law, a linear Goodman diagram and a bi-linear Goodman diagram. The former assumes that the S-N behavior is independent of mean stress and that the slope of the S-N curve is constant. The results illustrate the power law formulation is most conservative of the four formulations; namely, it produces the highest EFL and the shortest predicted service lifetimes. When compared to one another, the linear and bi-linear formulations yield essentially the same damage estimates, with the bi-linear formulation being slightly less conservative than the linear. For most cases, both the linear and the bi-linear formulations are conservative when compared to the detailed MSU/DoE formulation, depending on the nature of the load spectrum.

Thus, the MSU/DoE formulation of the Goodman diagram with a detailed representation of thirteen R values indicates that the effects of mean stress are more important than previously thought. The region where the composite is transitioning between compressive and tensile failure modes in particularly important and the updated Goodman diagram provides a better description of this region.

REFERENCES

1. Sutherland, H.J., 1999, *On the Fatigue Analysis of Wind Turbines*, SAND99-0089, Sandia National Laboratories, Albuquerque, NM, 132 p.

2. van Delft, D.R.V., G.D. de Winkel and P.A. Joosse, "Fatigue Behavior of Fiberglass Wind Turbine Blade Material Under Variable Amplitude Loading," *1997 ASME Wind Energy Symposium*, AIAA/ASME, pp. 180-188.

3. Nijssen, R.P.L, D.R.V. van Delft and A.M. van Wingerde, 2002 ASME Wind Energy Symposium, AIAA/ASME, pp. 10-18

4. J.F. Mandell, D.D. Samborsky, N.K. Wahl, and H. J. Sutherland, *Testing and Analysis of Low Cost Composite Materials Under Spectrum Loading and High Cycle Fatigue Condition*, ICCM14,

5. J.F. Mandell, and D.D. Samborsky, *DOE/MSU Composite Material Fatigue Database: Test Methods, Materials, and Analysis*, SAND97-3002, Sandia National Laboratories, Albuquerque, NM (1997).

6. J.F. Mandell, D.D. Samborsky, and D.S. Cairns, *Fatigue of Composite Material and Substructures for Turbine Blades,* SAND2002-077, Sandia National Laboratories, Albuquerque, NM (2002).

7. Sutherland, H.J., P.L. Jones, and B. Neal, 2001, "The Long-Term Inflow and Structural Test Program," *2001 ASME Wind Energy Symposium*, AIAA/ASME, pp. 162-172.

8. Sutherland, H.J., "Analysis of the Structural and Inflow Data from the LIST Turbine," *Journal of Solar Energy Engineering*, Transactions of the ASME, v. 124, November, 2002, pp. 432-445.

9. Mandell, J.F., D.D. Samborsky, N.K. Wahl, and H.J. Sutherland, *Testing and Analysis of Low Cost Composite Materials Under Spectrum Loading and High Cycle Fatigue Conditions*, Conference Paper, ICCM14, Paper # 1811, SME/ASC 10 p

10. J.F. Mandell, D.D. Samborsky, D.W. Combs, M.E. Scott and D.S. Cairns, *Fatigue of Composite Material Beam Elements Representative of Wind Turbine Blade Substructure*, NREL/SR-500-24374, National Renewable Energy Laboratory, Golden, Co (1998).

11. Sutherland, H.J., J.R. Zayas, A.J. Sterns and B. Neal, 2004, "Update of the Long-Term Inflow and Structural Test Program," *2001 ASME Wind Energy Symposium*, AIAA/ASME, in publication.

12. Kelley, N., M. Hand, S. Larwood, and E. McKenna, 2002, "The NREL Large-Scale Turbine Inflow and Response Experiment – Preliminary Results," *2002 ASME Wind Energy Symposium*, AIAA/ASME, pp. 412-426.

13. Sutherland, H.J., N.D. Kelley and M.M. Hand, "Inflow and Fatigue Response of the NWTC Advanced Research Turbine," *2003 ASME Wind Energy Symposium*, AIAA/ASME, 2003, pp. 214-224.

14. Jackon, K., Dynamic Design, Davis, CA and M. Zuteck, MDZ Consulting, Clear Lake Shores, TX, personal communication.

15. Malcolm, D., GEC, Kirkland, WA, personal communication.

16. Buhl, M.L., Jr, *CRUNCH User's Guide*, Ver. 2.61, NREL/NWTC, Golden, CO., 2001, 11 p.

17. Musial, W., M. Clark, N. Egging and M. Zuteck, 1997, "A Comparison of Strength and Load-Based Methods for Testing Wind Turbine Blades," 1997 ASME Wind Energy Symposium, AIAA/ASME, W. Musial and D.E. Berg, eds., p. 228.